THE JOURNAL OF PHYSICAL CHEMISTRY A

Article

pubs.acs.org/JPCA

Ion Mobilities in Diatomic Gases: Measurement versus Prediction with Non-Specular Scattering Models

Carlos Larriba* and Christopher J. Hogan, Jr.

Department of Mechanical Engineering, University of Minnesota, Minneapolis, Minnesota 55455, United States

Supporting Information

ABSTRACT: Ion/electrical mobility measurements of nanoparticles and polyatomic ions are typically linked to particle/ion physical properties through either application of the Stokes–Millikan relationship or comparison to mobilities predicted from polyatomic models, which assume that gas molecules scatter specularly and elastically from rigid structural models. However, there is a discrepancy between these approaches; when specular, elastic scattering models (i.e., elastic-hard-sphere scattering, EHSS) are applied to polyatomic models of nanometer-scale ions with finite-sized impinging gas molecules, predictions are in substantial disagreement with the Stokes–Millikan equation. To rectify this discrepancy, we developed and tested a new approach for mobility calculations using polyatomic models in which non-specular (diffuse) and inelastic gas-molecule scattering is considered. Two distinct semiempirical models of gas-molecule scattering from particle surfaces were considered. In the first, which has been traditionally invoked in the study of aerosol nanoparticles, 91% of collisions are diffuse and thermally accommodating, and 9% are specular and elastic. In the second, all collisions are considered to be diffuse and accommodating, but the average speed of the gas molecules reemitted from a particle surface is 8% lower than the mean thermal speed at the particle temperature. Both scattering models attempt to mimic exchange between translational, vibrational, and rotational modes of energy during collision, as would be expected during collision between a nonmonoatomic gas molecule and a nonfrozen particle surface. The mobility calculation procedure was applied considering both hard-sphere potentials between gas molecules and the atoms within a particle and the long-range ion–induced dipole (polarization) potential. Predictions were compared to previous measurements in air near room temperature of multiply charged poly(ethylene glycol) (PEG) ions, which range in morphology from compact to highly linear, and singly charged tetraalkylammonium cations. It was found that both non-specular, inelastic scattering rules lead to excellent agreement between predictions and experimental mobility measurements (within 5% of each other) and that polarization potentials must be considered to make correct predictions for high-mobility particles/ions. Conversely, traditional specular, elastic scattering models were found to substantially overestimate the mobilities of both types of ions.

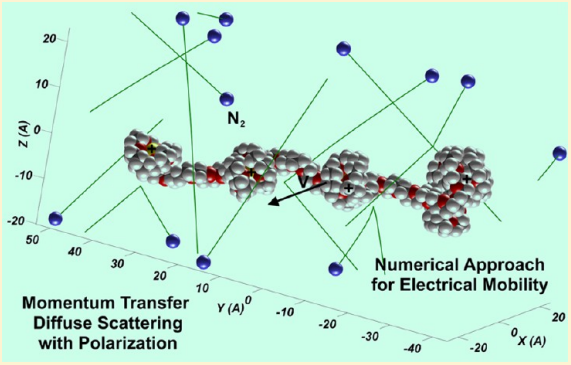

1. INTRODUCTION

One of the most commonly applied techniques for the physical characterization of nanometer-scale aerosol particles and macromolecular ions in diatomic background gases is separation based on electrical/ion mobility, Z_p.[1a,b] (In this work, the terms "particle" and "ion" are used generally to identify entities that are ionized and suspended in a background gas.) In atmospheric-pressure and reduced-pressure environments, nanometer-sized particles fall within the momentum-transfer-free molecular regime, in which ion mobility (i.e., the ratio of a particle's net charge to its scalar friction factor) is expressed as[2]

$$Z_p = \sqrt{\frac{\pi m_{red}}{8kT}}\frac{3ze}{4\rho_{gas}\Omega} \quad (1a)$$

where m_{red} is the reduced mass for the gas molecule and particle, k is the Boltzmann constant, T is the temperature, z is the integer number (positive or negative) of charges on the particle, e is the unit elementary charge, ρ_{gas} is the gas mass density, and Ω is the particle's collision cross section. Mobility measurements hence can be and often are used to calculate collision cross sections. Inferred collision cross sections are, in turn, often related to the physical characteristics of the measured particles by one of two distinct approaches: they are either (1) linked to the physical sizes of particles based on the assumption that particles are spherical with known densities,[3] or (2) compared directly to collision-cross-section predictions derived from calculations of gas-molecule scattering from the surfaces of polyatomic models.[4]

The present study is motivated by the fact that, although these two approaches have both been invoked in a large number of studies, they are not congruent with one another for

Received: December 17, 2012
Revised: February 14, 2013
Published: March 14, 2013

   dx.doi.org/10.1021/jp312432z | J. Phys. Chem. A 2013, 117, 3887–3901

mobility measurements made in diatomic gases, such as N_2 and air. In approach 1, commonly utilized in the measurement of the mobility of atmospheric aerosol particles,[3] following Epstein[5] and Fernandez de la Mora et al,[6] the collision cross section is expressed as

$$\Omega = \frac{\pi}{4}\xi(d_p + d_g)^2 \tag{1b}$$

where d_p is the particle mobility diameter, d_g is the effective gas-molecule diameter, and ξ is the gas-molecule−particle momentum-transfer coefficient.[7] When compared to measurements of relatively compact particles in air at temperatures near 300 K, use of $\xi = 1.36$ and $d_g \approx 3.0$ Å in eq 1b leads to inferred d_p values in excellent agreement (within 1−2%) with the particles' volume-equivalent diameters (defined from the known mass and bulk density for each particle),[8] down to $d_p \approx 1.3$ nm. With $\xi = 1.36$, mobility diameters are further in excellent agreement with expected diameters derived from electron microscopy or X-ray crystallography[9] in the >10-nm size range.

The value of ξ is nonetheless entirely empirical; originally, it was inferred from the semiempirical equation for the low-Reynolds-number drag on a spherical particle provided by Cunningham,[10] which was verified together with Millikan[11] and later by the Millikan oil drop experiments.[12] In this drag equation, commonly referred to as the Stokes−Millikan equation,[8a] a correction (the slip correction factor) is added to Stokes's law to allow for a dependence of the scalar friction factor on the Knudsen number (Kn, the ratio of twice the surrounding-gas hard-sphere mean free path to the sum of the gas molecule and particle diameters). The ion mobility of a spherical particle obeying the Stokes−Millikan drag relationship is expressed as[13]

$$Z_p = \frac{ze}{3\pi\mu(d_p + d_g)}\left(1 + \frac{2\lambda}{d_p + d_g}\left\{A_1 + A_2 \exp\left[-\frac{A_3(d_p + d_g)}{\lambda}\right]\right\}\right) \tag{2a}$$

where λ is the hard-sphere mean free path of the background gas; μ is the gas viscosity; and A_1, A_2, and A_3 are dimensionless constants derived from oil drop experiments.[13] Considering the free-molecular regime, in which $\lambda \gg d + d_g$ ($Kn \to \infty$) and noting that $\mu \approx {}^1/_2\lambda\rho_{gas}\bar{c}$, where $\bar{c}$ is the mean gas-molecule thermal speed, eq 2a can be written as

$$Z_p = \frac{4ze(A_1 + A_2)}{3\pi\bar{c}\rho_{gas}(d_p + d_g)^2} = \sqrt{\frac{\pi m_{gas}}{8kT}}\frac{ze}{\rho_{gas}}\frac{4(A_1 + A_2)}{3\pi(d_p + d_g)^2} \tag{2b}$$

In N_2 background gas, $A_1 + A_2 = 1.657$ agrees with experimental results nearly without exception,[8f,9a,13,14] and comparison of eq 2b to eqs 1a and 1b yields a value for ξ of

$$\xi = \frac{9}{4(A_1 + A_2)} = 1.3578 \tag{3}$$

In contrast with experimentally derived approach 1, approach 2 is typically invoked when comparing the collision cross sections predicted for structures of biomolecules in the gas phase to measured collision cross sections[4,15] and where implemented collisions between gas molecules and particles have been overwhelmingly modeled as elastic and specular. Although specular scattering model predictions are in reasonable agreement with mobility measurements made in monatomic He background gas on small ions (masses less than 2 kDa),[16] modeling collisions as specular and elastic with a smooth convex surface yields $\xi = 1$ and, when applied to most polyatomic models, leads to $\xi < 1.36$.[16a] For this reason, elastic, specular scattering predictions agree with neither the Millikan drag measurements[12a] nor the findings of recent studies on nanometer-scale entities in diatomic background gases,[8a] which are in line with $\xi = 1.36$. The purpose of this study was hence to develop and test a new approach for mobility/collision-cross-section calculations for polyatomic models of entities in the gas phase that leads to predictions in better agreement with measurements in diatomic gases and does so using models for both particles and gas molecules scaled from independent experimental measurements (i.e., nonmobility measurements). Non-specular, inelastic scattering of gas molecules is considered in this approach, leading to values in agreement with $\xi = 1.36$ for spherical particles when the mobility diameter is equated with the volume-equivalent diameter. In the sections that follow, the calculation procedure is partially described, and predictions of collision cross sections are compared to experimental measurements of the collision cross sections of poly(ethylene glycol)[17] and tetraakylammonium[18] ions measured in air, either considering hard-sphere potentials or accounting for ion−induced dipole potentials between particle and gas molecule.

2. THEORY AND NUMERICAL ALGORITHMS

2.1. Overview of Collision-Cross-Section Calculations.

Collision-cross-section/mobility calculations hinge on the determination of the amount of momentum transferred from gas molecules to a particle in the presence of net flow between the gas and particle. The numerical procedures invoked in calculations are described in greater detail in a companion report;[19] in this work, we are concerned with testing the ability of calculation procedures to predict the correct collision cross sections from structural models.

With recent exceptions,[20] collision-cross-section calculations from polyatomic models in prior studies have primarily relied on the MOBCAL suite of algorithms,[4,15a] in which the collision cross section can be determined in three different manners: (1) calculation of the orientationally averaged projected area of a particle and the assumption that this area is exactly equal to the collision cross section [the projected-area (PA) method]; (2) calculation of the collision cross section with the assumption that a monatomic, specular, elastic scattering molecule impinges onto a particle structure composed of hard-sphere atoms [the elastic-hard-sphere scattering (EHSS) method];[16a] and (3) calculation of the collision-cross-section monitoring gas-molecule trajectories, considering Lennard-Jones interactions (with the possibility of other interactions)[21] between a spherical gas molecule and the atoms within a particle [the TM method].[22] In the latter two methods, the momentum-transfer integral is simplified based on the approach employed by Mason and McDaniel.[2] Distinct from Mason and McDaniel's approach, we replace the momentum integral simplification with a full Maxwell−Boltzmann distribution approximation where gas molecules can approach and impinge on a particle from all directions,[23] mimicking a Maxwell−Boltzmann gas ensemble. This mode of calculation has the advantage of being able to reproduce real gas conditions and allows for the possibility of accounting for gas-molecule−gas-

dx.doi.org/10.1021/jp312432z | J. Phys. Chem. A 2013, 117, 3887−3901

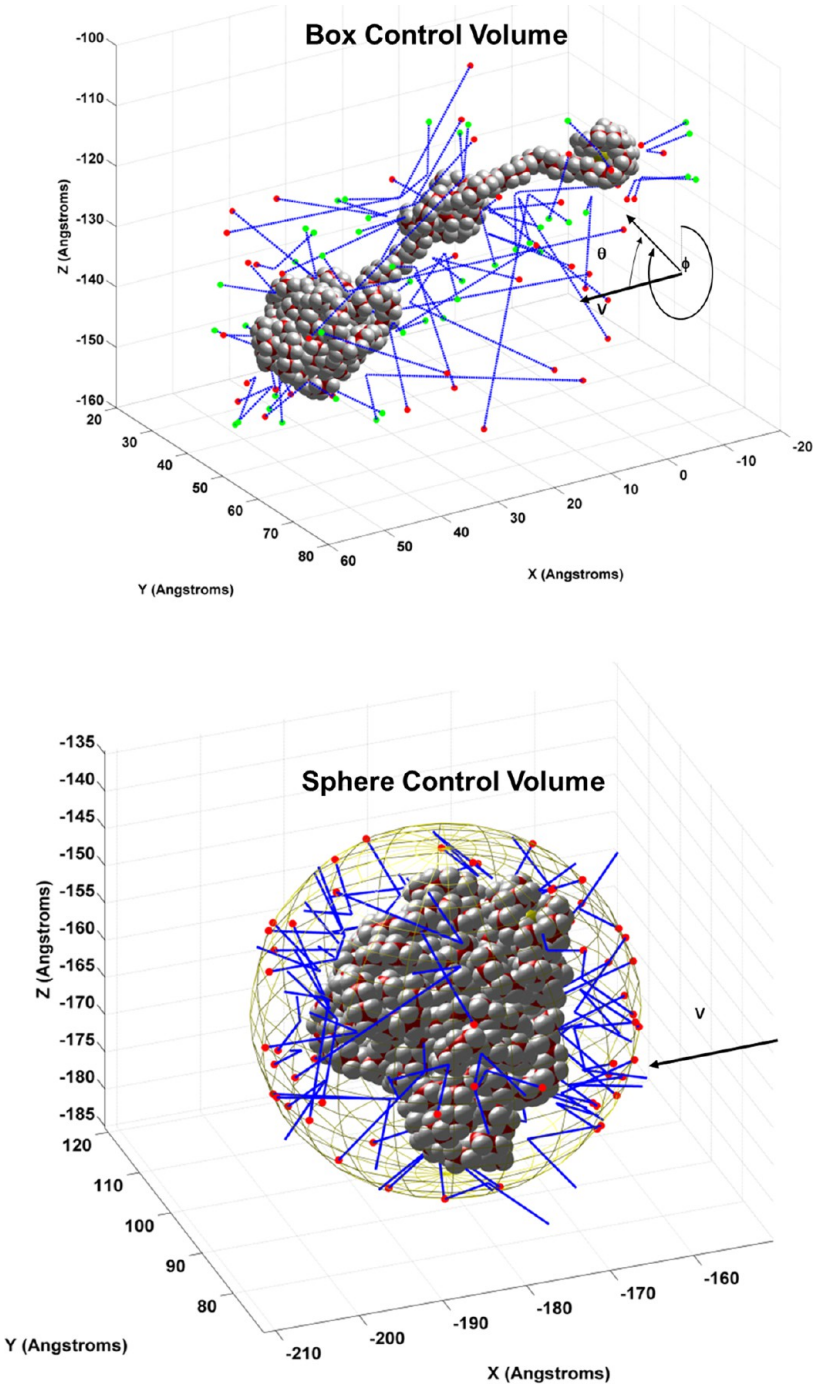

Figure 1. Examples of the box (upper pane, containing a stretched poly(ethylene glycol) 115-mer) and sphere (lower pane, containing a compact poly(ethylene glycol) 254-mer) control volumes used in collision-cross-section calculations. Sample trajectories for hard-sphere gas molecules introduced into both control volumes and impinging with the examined particle structures are displayed. The inclination and azimuthal angles, θ and ϕ, respectively, are also displayed in the upper pane.

molecule collisions, which would become important for large-scale simulations when the particle in question is similar in size to the hard-sphere gas-molecule mean free path (at finite *Kn*).[24] More important for the present study, the examination of gas-molecule impingement from all directions also enables the formation of a symmetric drag tensor when any three perpendicular directions for the orientation of the flow are considered.[25] Therefore, calculations with no more than three orientations are needed to determine the collision cross section (orientationally averaged) of any particle.

The collision-cross-section/mobility calculation procedure can be broken down into two steps: (1) introduction of the gas molecule into the simulation control volume and (2) determination of the degree of momentum exchange between the gas molecule and particle upon gas-molecule impingement. Calculations are further broken down into instances where no long-range potential interaction exists between the gas molecule and particle (i.e., hard-sphere potentials) and those where an ion−induced dipole (polarization) potential is considered. In the latter case, momentum transfer occurs not only upon

dx.doi.org/10.1021/jp312432z | J. Phys. Chem. A 2013, 117, 3887−3901

collision but also when gas-molecule trajectories are altered by close approach to a particle. We first discuss the introduction of gas molecules into the control volume, followed by momentum-transfer calculations for gas molecules in the absence of polarization, and finally the incorporation of long-range potentials into momentum-transfer calculations. In all instances, a structural (polyatomic) model of both the particle and gas molecule (treated as a sphere in this work, although intended to mimic a diatomic gas molecule in the manner in which it behaves during a collision) are required. Further, to improve the computational efficiency over other recently developed algorithms used to predict collision cross sections in diatomic gases,[26] all atoms are modeled as spheres with prescribed radii. It is therefore critical that the sizes of the spheres used in the model are reasonable for the gas molecule[27] and the atoms within the particle at the temperature under examination, as the use of incorrectly sized atoms will influence results. However, with appropriately selected radii, we suggest that predictions from this approach will match experimental calculations, without the need of modeling atoms with Lennard-Jones potential interactions.[26,28]

2.2. Introduction of Gas Molecules into the Control Volume. A common approach in prior theoretical analyses[5,29] of free-molecule mobility/momentum-transfer calculations has been to determine the number of impinging molecules per unit time on a surface element of a particle. Calculation of the momentum transfer of impinging molecules on the particle per unit time integrated over the whole surface area of the particle will give the total drag caused by bulk motion and, hence, the particle's collision cross section. Although this approach is easy to implement when the surface area of the particle is convex and not complicated (see the Supporting Information for this procedure applied to a sphere), it becomes rather burdensome as the exterior becomes increasingly corrugated and concave (e.g., the surface of a molecule). A more convenient approach, employed here, is to calculate the momentum flux of gas molecules through simplified surfaces that form the boundaries of a control volume surrounding the particle. During ion-mobility measurements, a particle must be traveling at a speed V through a medium. The control volume used for calculation is set on the particle itself so that the bulk motion of the gas has a component in the direction of the velocity vector $\vec{V}$ to account for this speed. In the absence of this net velocity, gas molecules would enter the control volume following a Maxwell–Boltzmann velocity distribution

$$\rho_0 = \left(\frac{m_{gas}}{2\pi kT}\right)^{3/2} \exp\left[-\frac{m_{gas}(u^2 + v^2 + w^2)}{2kT}\right] \tag{4}$$

where ρ denotes the three-dimensional velocity distribution function;[30] the subscript 0 denotes the absence of bulk flow; and u, v, and w are the Cartesian components of the gas-molecule velocity vector. The incoming velocity distribution function, however, is skewed because of the particle's bulk motion. Defining the most probable speed as $h = (2kT/m_{gas})^{1/2}$ and $\vec{c}_{gas}$ as the gas-molecule velocity vector, the dimensionless velocity distribution in the presence of flow, $\rho^* = \rho h^3$, can be written as

$$\rho^* = \frac{1}{\pi^{3/2}} \exp(-\| \vec{c}^*_{gas} - \vec{V}^* \|^2) \tag{5a}$$

where the asterisks (*) denote vectors normalized by h. Equation 5a can be simplified, using both the assumption that the ratio of the speed of bulk motion to the mean thermal speed is small (low Mach number, which is valid in most linear mobility spectrometers) and the identity

$$\exp(x) = \sum_{n=0}^{\infty} \frac{x^n}{n!} \tag{5b}$$

Substituting this series into eq 5a and truncating the resulting infinite series after the first two terms yields

$$\rho^* = \frac{1}{\pi^{3/2}} \exp[-(\vec{c}^{*\,2}_{gas} + \vec{V}^{*2} - 2\vec{c}^*_{gas}\cdot\vec{V}^*)]$$
$$\approx \rho_0^* + 2(\vec{c}^*_{gas}\cdot\vec{V}^*)\rho_0^* = \rho_0^* + \rho_1^* \tag{6}$$

wherein $\vec{V}^{*2}$ is negligibly small in comparison to $\vec{c}^{*2}_{gas}$. With this linearization, the incoming gas-molecule velocity distribution is expressed as the sum of two subdistributions. The first of these, ρ_0^*, corresponds to the regular Maxwell–Boltzmann distribution and, by itself, leads to zero momentum transfer. Therefore, it can be neglected in some computations, and gas molecules enter the control volume following a distribution given by $\rho_1^* = 2(\vec{c}^*_{gas}\cdot\vec{V}^*)\rho_0^*$. Although the use of only ρ_1^* dramatically accelerates computations, the term $\vec{c}^*_{gas}\cdot\vec{V}^*$ can lead to gas molecules entering the domain with "negative" momentum, which must be taken into account in calculations. The method by which these negative gas molecules are handled is discussed in the companion report[19] and not examined further here.

With hard-sphere potentials, if the control volume is too large compared to the particle, many of the sampled gas molecules will exit the volume without impingement; thus, they will not transmit any momentum. This unnecessarily increases computation time. Conversely, calculation of the size and shape of the optimum control volume and the proper distribution of entering gas molecules on the control surface is a nontrivial problem. We hence used either a sphere or a rectangular box as the control volume, with examples of both portrayed in Figure 1. The upper pane of Figure 1 displays the structure of poly(ethylene glycol) (PEG) ion (particle) with four excess positive charges (modeled by cesium ions) and 115 monomer units, as determined by molecular dynamics (ChemBio3D, MM2 force field). Coulombic repulsion between excess charges drives the PEG chain to adopt a bead-string-like structure where one larger end bead holds two of the excess charges and the smaller two beads each hold one excess charge.[17] Because of this semielongated structure, calculation of the collision cross section for this chain is best performed using a rectangular box-shaped control volume. Conversely, in the lower pane of Figure 1, a PEG chain with 254 monomer units is shown, which, also with four excess positive charges, adopts a more compact structure with minimal Coulombic stretching.[17] In this instance, as the chain collapses to a near-spherical structure, a spherical control volume is used in the calculation. To efficiently determine whether a rectangular box or sphere should be used for collision-cross-section calculations, we found the dimensions (length, width, and height for the box or diameter for the sphere) for the smallest box and sphere capable of entirely encasing the entire structure under consideration. The shape requiring the smaller volume to enclose the particle was selected as the control volume, with the specified dimensions.

When a box is the appropriate control volume choice, one of its faces is aligned with the velocity vector, e.g. $\vec{V} = V\hat{i}$. The gas-molecule flux (volumetric flow rate, Q per unit area, A) that crosses any given side of the box is given by the equation

dx.doi.org/10.1021/jp312432z | J. Phys. Chem. A 2013, 117, 3887–3901

$$Q/A = h \int_{\vec{c}^*_{gas}\cdot\vec{n}<0} \rho_1^*(\vec{c}^*_{gas}\cdot\vec{n})\, du^*\, dv^*\, dw^* \qquad \text{(box)} \tag{7a}$$

where $\vec{n}$ is the unit outward normal to the surface of the control volume, $\vec{c}^*_{gas}$ is the velocity vector for a gas molecule, and the gas molecules that account for the flux into the control volume are those for which $\vec{c}^*_{gas}\cdot\vec{n} < 0$. Gas molecules for which $\vec{c}^*_{gas}\cdot\vec{n} > 0$ are exiting the control volume and were omitted from calculations. For a spherical control volume, it is similarly necessary to differentiate between gas molecules entering the control volume and those exiting. With $\vec{n}$ again defined as the unit outward normal, the flow rate of gas molecules coming into the sphere can be expressed as

$$Q = 2h \int_{\vec{c}^*_{gas}\cdot\vec{n}<0}^{\vec{V}^*\cdot\vec{c}^*_{gas}<0} \rho_1^*(\vec{c}^*_{gas}\cdot\vec{n})\, du^*\, dv^*\, dw^*\, \delta A \qquad \text{(sphere)} \tag{7b}$$

In this equation, only the positive volumetric rate, which depends on the positions of the incoming gas molecules as well as on its incoming angle (requiring the flow rate to be expressed in an integral form over the surface area of the sphere), is considered ($\vec{V}^*\cdot\vec{c}^*_{gas} < 0$), as the total volumetric rate through the spherical surface (positive and negative) will always add up to 0.

Irrespective of whether a gas molecule introduced into the control volume impinges on the particle, it inevitably exits the control volume. The drag force (momentum transferred from the gas molecules to the particle per unit time, in the direction of the bulk flow), $\vec{F}_D$, brought about by all gas-molecule collisions is calculated as

$$\vec{F}_D = \frac{h m_{gas}}{t_T}(\vec{I} - \vec{I}_r) \tag{8a}$$

with

$$\vec{I} = \sum_{i=1}^{M} \bar{s}^*_{0,i}\hat{v}_{0,i} \tag{8b}$$

and

$$\vec{I}_r = \sum_{i=1}^{M} \bar{s}^*_{r,i}\hat{v}_{r,i} \tag{8c}$$

where M is the total number of collision events occurring for N sampled gas molecules. A collision event is defined as an instance in which the velocity vector of an introduced gas molecule changes during the simulation, which requires collision in the absence of gas-molecule−particle potential interactions. Collision/impingement, in turn, is specifically defined as an instant in which a gas molecule takes a trajectory that leads to its arrival at a location at the most a distance of $r_g + r_a$ from any atom within a particle's structure, where r_g is the gas-molecule radius and r_a is the radius of the atom. When the gas molecule arrives at this location, the collision rules employed in the simulation, discussed in the subsequent section, must be invoked.

Also in eqs 8a−8c, t_T is the time necessary for the N emitted molecules to go through the surface of the control volume; $\bar{s}^*_{0,i}$ and $\bar{s}^*_{r,i}$ are the speeds of the gas molecule as it enters and leaves the control volume, respectively (scalars, nondimensionalized by h); and $\hat{v}_{0,i}$ and $\hat{v}_{r,i}$ are the respective entering and leaving gas-molecule unit velocity vectors. The subscript i denotes the ith collision event. t_T is an input and is linked to the number of sampled particles as well as the flux through each portion of the control volume surface. With the flow rate through a wall of the box calculated using eq 7a, N_w, the number of sampled gas molecules through a particular face of the box, is determined as

$$N_w = (\rho_{gas}/m_{gas})Qt_T \tag{9}$$

The total number of sampled gas molecules is the sum of the N_w values for all box faces ($N = \sum N_w$), and similarly, M_w is the sum of all collision events from each face. Therefore, t_T must be chosen sufficiently large to minimize statistical dispersion in the calculation results. Alternatively, N can be chosen as a program input, as statistical convergence depends purely on the number of collision events examined. With N selected, t_T can be calculated with eq 9, provided that, for each face of the box, N_w values are chosen in proportion to the volumetric flow rate of gas molecules through each face.

The position at which a sampled gas molecule is placed on a particular face is random, while the angles (θ and ϕ, indicated in Figure 1) defining the direction of gas molecule's initial velocity vector ($\hat{v}_{0,i}$)) are chosen from probability distributions based on 7.[19] On the front and back faces of the box (which are perpendicular to the bulk flow), the inclination angle θ represents the deviation from the positive (or negative) x direction up to $\pi/2$, allowing only those molecules that satisfy $\vec{c}^*_{gas}\cdot\vec{n} < 0$ to be considered. It is selected using the equation[31]

$$\cos(\theta) = R_1^{1/3} \tag{10a}$$

where R_1 is a uniformly distributed random variable between 0 and 1. The azimuthal angle ϕ ranges from 0 to 2π, and on the front and back faces of the box it is selected with the equation[31]

$$\phi = 2\pi R_2 \tag{10b}$$

where R_2 is also a uniformly distributed random variable between 0 and 1. For the box faces parallel to the flow, θ and ϕ are determined from the equations[31]

$$\sin(\theta) = R_1^{1/3} \tag{10c}$$

$$\sin(\phi) = 2R_2 - 1 \tag{10d}$$

$$\cos(\phi) = \text{sign}(2R_3 - 1)[1 - \sin^2(\phi)]^{1/2} \tag{10e}$$

In the absence of gas-molecule−particle potential interactions, the value of the computed drag can be found without accounting for the gas-molecule speed distribution. Therefore, the dimensionless initial speed $\bar{s}^*_{0,i}$ is chosen as the average velocity

$$\bar{s}^*_{0,i} = \frac{\int_0^\infty 2V^* s^5 e^{-(s^2)}\, ds}{\int_0^\infty 2V^* s^4 e^{-(s^2)}\, ds} = \frac{8}{3\sqrt{\pi}} \tag{10f}$$

Whenever a correctly sampled speed is desired, the procedure reported by Chan and Dahneke[32] can be employed. Finally, the initial positions, angles, and speeds for gas molecules on a sphere must be similarly calculated when a spherical domain is used; the equations invoked to select these angles are provided elsewhere.[19]

2.3. Momentum Exchange upon Gas-Molecule Impingement. In instances where the gas-molecule trajectory is rectilinear (as is the case in the absence of long-range potential interactions, depicted in Figure 1) and the gas molecule

dx.doi.org/10.1021/jp312432z | J. Phys. Chem. A 2013, 117, 3887−3901

impinges on the particle surface, we determine the reemission angle and velocity (i.e., the trajectory of the gas molecule after the collision) through a specified set of collisions rules described in greater detail elsewhere.[19] After reemission, the collision check is again performed, and the process is repeated until the gas molecule exits the control volume. Provided that a collision event and momentum exchange occur, the change in gas-molecule momentum from the beginning to the end of the calculation is incorporated into the drag force calculation (eq 8a). The drag force is linearly related to the bulk velocity V when t_T is introduced into eq 8a, and the collision cross section/ion mobility is therefore independent of the speed of bulk motion. Supposing that all particle orientations are equally probable, a dimensionless drag tensor, [B], can be constructed by calculating the force produced by the bulk flow in three different perpendicular directions. The components of this tensor, $B_{\chi\omega}$, are determined as

$$B_{\chi\omega} = I_{\chi\omega} + I_{r_{\chi\omega}} \tag{11}$$

where χ refers to the direction in which the bulk velocity vector is aligned (e.g., when $\chi = x$, $\vec{V} = V\hat{i}$) and ω refers to the component (x, y, or z) of the vectors $\vec{I}$ and $\vec{I}_r$ determined when the velocity vector is aligned in the χ direction. We note that the actual orientation of the particle within the control volume does not influence the result, provided that the momentum-transfer calculations are performed in three separate perpendicular directions. The tensor [B] will be symmetric and positive-definite; hence, it can be diagonalized as explained by Happel and Brenner.[25] After diagonalization, leaving only the components B_{xx}, B_{yy}, and B_{zz} with nonzero values, the ion mobility of the particle under consideration is determined as

$$Z_p = \left(1 + \frac{m_{gas}}{m_p}\right)^{1/2} \frac{\sqrt{\pi}zet_T}{8m_{gas}}\left(\frac{1}{B_{xx}} + \frac{1}{B_{yy}} + \frac{1}{B_{zz}}\right) \tag{12}$$

where the term $[1 + (m_{gas}/m_p)]^{1/2}$ is introduced to account for the influence of finite particle mass.[8b] To determine a specific ion mobility, which varies not only with particle properties but also with background gas conditions, the net particle charge, gas-molecule mass, gas density, and temperature are required inputs, with the latter three parameters input into calculations (along with t_T and $\vec{V}$, which are calculation inputs but do not influence the result, provided that t_T is sufficiently long). The collision cross section, in turn, can be calculated from Z_p using eq 1a.

With this calculation procedure in place, what remains is to develop a model for the collision and reemission of gas molecules that gives rise to the results observed in diatomic gases. To most accurately simulate gas-molecule reemission, it would be necessary to analyze collisions between a rotating, vibrating, and translating diatomic gas molecule with a rotating, vibrating, and translating (locally) atom in the particle. Such an analysis, although not impossible, is very computationally expensive and theoretically cumbersome. The existence of translational, vibrational, and rotational motion, however, should lead to an increase in the drag on a particle moving relative to a gas over the amount of drag in the presence of whole-particle and gas-molecule translational motion only. Indeed, it is highly likely, albeit unproven, that their existence leads to the experimental observation of $\xi = 1.36$ into the nanometer scale. There is therefore a need to effectively account for energy exchange upon collision in the mobility model, but without modeling the motion of all atoms involved in such detail.

Although overlooked in many recent reports on predictions of ion mobility,[4,16a,20,22] there were several early attempts to effectively account for translational, rotational, and vibrational energy exchange upon collision, initially by Langevin[33] and Lenard,[34] without completely modeling the motion of individual atoms. Accounting for these multiple forms of kinetic energy while treating colliding entities as hard spheres with a fixed particle structure requires the following conditions: (1) relaxation of the assumption of elastic and specular collisions, (2) allowance for gas-molecule reemission from a particle surface at non-specular (diffuse) angles, and (3) allowance for changes in gas-molecule translational energy after collision (energy accommodation/inelasticity). Notably, Epstein[5] analyzed several possible modes of gas-molecule reemission upon impingement from a particle surface along these lines, considering both specular and diffuse reemission angles as well as elastic and inelastic reemission speeds.[38] Based on this analysis, through comparison to experimental measurements, he concluded that most gas-molecule–particle collisions are effectively wholly diffusive, with the gas-molecule reemission angle random and independent of the impingement angle and with complete energy accommodation; that is, the gas-molecule translational energy upon reemission is in equilibrium with the internal energy (vibrational, rotational, and atomic translational energy) of the particle, so that the gas-molecule reemission speed is sampled from a Maxwell–Boltzmann distribution at the particle temperature. To specifically match the Millikan oil drop experimental results and arrive at $\xi = 1.36$ with Epstein's diffuse-accommodating collision model, approximately 91% of gas-molecule–particle collision events should be diffuse and energy accommodating, with the remaining 9% of collisions specular and elastic (as the diffuse-accommodating collisions alone lead to $\xi = 1 + \pi/8 = 1.392$ and specular collisions from a smooth surface lead to $\xi = 1.00$).

The 91% diffuse-accommodating collisions, 9% specular-elastic collisions model is normally accepted within the field of aerosol science as a plausible explanation of the Millikan oil drop experiments,[35] with some arguing that the percentage of diffuse-accommodating collisions decreases with particle size.[27b,36] However, this theoretical framework is by no means unique in its ability to explain experimental observations, and indeed some issues arise when assuming that gas-molecule–particle collisions behave as described by Epstein. Beyond the agreement with measurements of drag coefficients/mobility, there is no other evidence supporting the idea that 91% of collisions are diffuse and accommodating irrespective of the chemical composition of the particle. It is further unlikely that gas-molecule–particle collisions are one of two types that are so distinct from one another in the reemission angular distribution (completely random or deterministic) and the degree of energy accommodation (completely accommodating versus completely elastic). On the contrary, it is more likely that collisions are of a single type, with continuous distributions in both the reemission angle and the speed of the gas molecule after collision. These distributions could certainly be functions of the sizes and shapes of both the gas molecule and particle, but until detailed molecular dynamics simulations of particle–gas-molecule collisions are performed,[37] they will remain ambiguous.

In light of these uncertainties, we present for comparison an additional collision model that leads to $\xi = 1.36$ when applied to spherical particles, but note that this collision model is by no means exact at the fundamental level and that numerous alternative models can be developed for this purpose. Our choice of collision model is simply brought about by the need to have an easily implementable algorithm to use in collision-cross-section calculations (that lead to accurate predictions) and to show that experimental results can be explained by a collision model distinct from the 91% diffuse-accommodating collisions, 9% specular-elastic collisions model. Specifically, in this collision model, all collisions are considered to behave similarly; gas molecules, approximated as spheres, have random Maxwell−Boltzmann-distributed instantaneous reemission angles independent of their impingement speed; and the reemitted gas molecules have all been accommodated such that their average translational speed can be determined from a Maxwell−Boltzmann distribution with a most probable speed 8% lower than expected at the temperature of the particle. Therefore, the "accommodation coefficient" is considered to be 100% as opposed to 91%, and this model effectively mimics an exchange from the translational energy of an impinging gas molecule into atomic translational energy within the particle or into vibrational and rotational energy within both the gas molecule and the particle. Although this treatment of collisions can certainly be improved, as it suggests that the internal energy of a particle moving in a background gas increases each time a gas molecule impinges on it, it is a simple approximation that is in line with eqs 1a and 1b and experimental measurements. As shown in the Supporting Information, when applied to a smooth sphere moving through a bath gas composed of negligibly small molecules, this model indeed leads to $\xi = 1.36$.

2.4. Modifications for Polarization Potentials. Although we contend that collision-cross-section predictions using hard-sphere and Lennard-Jones interpretations of atoms should not differ from one another substantially provided that the radii of atoms are chosen appropriately for the temperature of interest, when considering migration of a charged particle through a diatomic gas, it is still necessary to incorporate the influence of particle−gas-molecule potential interactions. Diatomic gas molecules have non-negligible polarizabilities;[38] thus, when approaching a particle, they have trajectories that can be influenced by longer-range polarization potentials if the energy of this potential approaches the thermal energy at the particle surface. For singly charged entities in air, N_2, or even higher-polarizability gases, polarization potentials can significantly influence the mobilities of particles that are ∼1.3 nm in characteristic size (diameter) and smaller,[8a,b] whereas for multiply charged entities introduced into the gas phase by electrospray, polarization can affect the mobilities of even larger-sized entities.[39]

When a gas molecule is a distance r_i from a net charge ze, the polarization energy, U_{pol}, is given by the equation

$$U_{pol} = -\frac{\alpha z^2 e^2}{8\pi\epsilon\epsilon_0 r_i^4} \tag{13a}$$

where α is the polarizability of the background gas molecules (∼1.7 Å^3 in air, N_2, and O_2), ε_0 is the permittivity of free space, and ε is the dielectric constant of the background gas. Correspondingly, the force brought about by this potential, F_{pol}, is given by the equation

$$F_{pol} = -\nabla U_{pol} \tag{13b}$$

In instances where a distribution of excess charge is present within the particle structure, the polarization force experienced by a gas molecule is calculated as the sum of the individual forces brought about by each present charge. The mobility/collision-cross-section calculation procedure described in sections 2.2 and 2.3 was modified to account for the polarization potential by (1) moving gas molecules within the control volume using the velocity Verlet algorithm,[40] (2) sampling incoming gas-molecule speeds and angles into the control volume from the skewed Maxwell−Boltzmann speed distribution[32] (i.e., replacing eq 10f with a random sampling from the distribution $\rho_0^* + \rho_1^*$),[19] and (3) enlarging the control volume so as to correctly determine all incoming gas-molecule trajectories. For the last modification, when a box was used as the control volume, the walls were positioned at least 2 nm from the center of any excess charge (for room-temperature calculations), so that, for N_2, the ratio of the polarization energy to the mean thermal energy (kT) was always less than 0.002 on any boundary. The use of a volume larger than prescribed by this criterion was found to have no influence on the calculation results and only reduced the computation speed. Spherical control volumes were similarly enlarged when polarization potentials were considered. For the velocity Verlet algorithm, we employed a variable-dimensional time step of around 1 fs, which was found to be accurate for calculations around 300 K in diatomic gases. Gas-molecule trajectories were monitored until collision, where the indicated collision rules were used to determine the gas-molecule reemission angle and speed. As with hard-sphere calculations, gas-molecule motion was monitored until a gas molecule left the control volume. The dimensionless scalar speeds ($\bar{s}_{0,i}^*$ and $\bar{s}_{r,i}^*$) and directional vectors ($\hat{v}_{0,i}$ and $\hat{v}_{r,i}$) of sampled gas molecules as they entered (subscript 0) and left (subscript r) the control volume were again used to calculate the mobility. Aside from the the sampling of the Maxwell−Boltzmann speed distribution, the procedure used to initially seed gas molecules on the control volume surface did not change. However, unlike in the case of hard spheres, in which some gas molecules exit the control volume without collision and do not transfer any momentum, in the presence of polarization potentials, all gas molecules transfer momentum, even those that do not collide (termed "grazing" collisions). Therefore, the number of collision events (M) is exactly equal to the number of sampled gas molecules (N) when potentials are considered.

3. RESULTS AND DISCUSSION

3.1. Test Cases and Determination of Candidate Structure Morphology. We compared predictions of the presented calculation procedure to mobility measurements of multiply charged PEG ions[17] and singly charged tetraalkylammonium ions,[18] all made in air using high-resolution differential mobility analysis (DMA).[1a,41] Calculations were performed with both the 91% diffuse-accommodating, 9% specular-elastic collision model and the proposed diffuse scattering model with an 8% reduction in the reemission speed with and without including polarization potentials. In this work, calculations performed with either of these scattering rules are henceforth referred to as DHSS (diffuse-hard-sphere scattering) methods. We further compared the results of DHSS methods to predictions assuming that gas-molecule scattering is specular and elastic, analogous to EHSS predictions but with gas

dx.doi.org/10.1021/jp312432z | J. Phys. Chem. A 2013, 117, 3887−3901

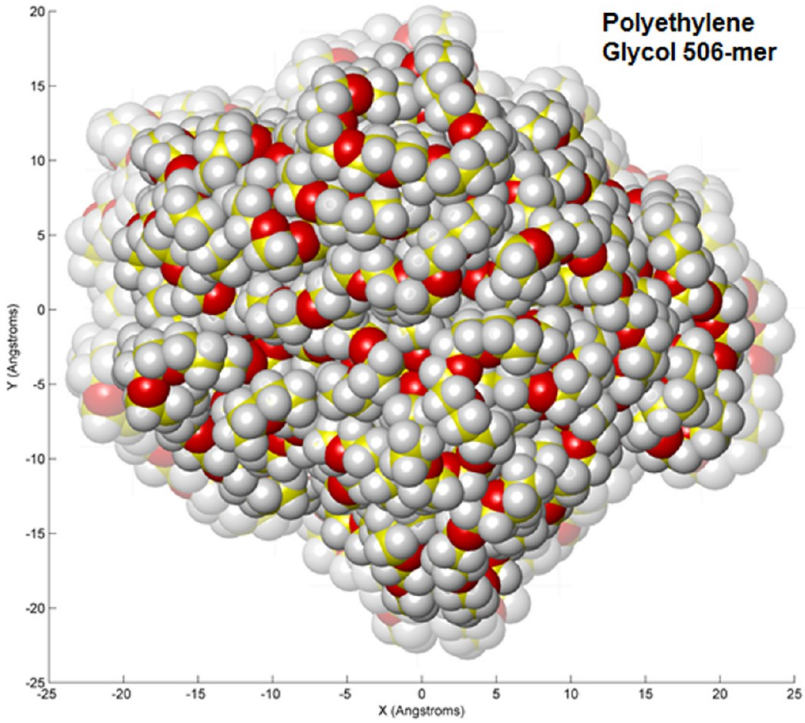

Figure 2. Collapsed structure of a poly(ethylene glycol) 506-mer (3545 atoms) rescaled such that its density agrees with the bulk value of poly(ethylene glycol).

molecules of finite sizes (as opposed to infinitesimal sizes) and the approximation that the orientationally averaged projected area of an entity is equivalent to its collision cross section (the PA approximation).[15a] For the reported predictions, we examined momentum transfer in each perpendicular direction for more than 10^5 gas molecules when polarization was neglected (~0.1−0.3% accuracy) and more than 10^6 gas molecules when it was considered. In all cases, we modeled the impinging gas molecules after molecular nitrogen, noting that molecular oxygen differs only slightly in physical dimensions, and in calculations, we treated each gas molecule as a sphere with a radius of 1.55 Å (d_g = 3.1 Å). Such spheres have projected areas equivalent to the orientationally averaged projected area of N_2 structures described by Niwa et al.,[27a] who modeled N_2 molecules as connected spheres with radii of 1.335 Å and a bond distance of 0.980 Å. Further, this value for the N_2 diameter seems to be in excellent agreement with the d_g values inferred/used in a number of recent measurements.[7,8,17,39a,c,41b,42]

We specifically chose the two aforementioned data sets for comparison not only because they contain singly and multiply charged ions in a wide mass range (up to ~12 kDa), but also because the measured entities have structures that can be predicted with little ambiguity, theoretically as well as experimentally. In the case of PEG ions, for which numerous ion-mobility measurements have been made,[8d,43] recent work[17] clearly reveals that the gas-phase structures observed are a function of the square root of the PEG ion mass, m_p, and the net number of excess charges, z. Beyond a critical value of $m_p^{1/2}/z$, PEG ions adopt collapsed structures, with densities close to the bulk PEG density. As $m_p^{1/2}/z$ decreases below this limit, more elongated PEG ions are observed (such as in the upper pane of Figure 1). This elongation process is reasonably well-understood,[17,43b,44] and correspondingly, the observed elongated structures have been well described, such that the structures of PEG ions can be determined well using molecular dynamics (MD) with a priori knowledge of the ion's mass and number of excess charges. Conversely, singly charged tetraalkylammonium ions, often used as mobility standards in the aerosol field,[8b,18,45] have structures that have been less studied in the gas phase than PEG ions. However, because of their limited degrees of conformational freedom, we believe that MD predictions can be used to create reasonable approximations for the structures of these ions as well.

MD simulations to generate PEG and tetraalkylammonium ion candidate structures were performed for this work using the ChemBio3D software package (version 11.0) with the MM2 force field.[46] For mobility calculations, it is essential that simulations converge to structures that are suitable not only in terms of their morphologies (e.g., stretched versus compact configurations), but also in terms of their absolute sizes (volumes). Although MM2 molecular mechanics are frequently used for the study of organic molecules, structures generated with this approach have anomalously low densities compared to expected values (although other molecular modeling approaches can be used that provide better agreement with expected densities[47]). A means of determining the appropriate volumes/radii of all atoms within simulated structures is hence required, such that the sizes of structures can be appropriately scaled prior to mobility calculations. We propose that correctly sized candidate structures for PEG ions can be generated by performing an MM2 simulation on a sufficiently large, low-charge-state entity of known chemical composition, which should have a density in line with the bulk density. To calibrate candidate structure sizes, simulations were performed using unperturbed MM2 force-field parameters; however, following simulations, the linear dimensions of the generated candidate structures and the radii of the atoms within structures were rescaled. Mobility calculations were performed using the rescaled candidate structures.

As suitable large, low-charge-state ions, we chose to examine two PEG chains, the first composed of 254 repeating units containing four Cs^+ ions (representing the excess charge) and the second consisting of an uncharged PEG ion with 506 repeating units. For both test chains, MD simulations were performed by initiating PEG structures as completely linear with no solvent present and, for the charged PEG chain, with four excess charges spaced evenly from one another on the PEG chain. A fixed temperature of 304 K (the temperature at which measurements were made[41b]) was employed, and after 400 ps of simulation time, both PEG structures remained close to fixed, although thermal energy permitted some structural variation between all accessible configurations at equilibrium. (A video showing the folding of the 506-repeating-unit PEG chain is provided in the Supporting Information.) A characteristic structure adopted by this PEG chain during simulation of the 506-repeating-unit chain is shown in Figure 2. In the case of PEG 254 with four Cs^+ charges, as the strength of electrostatic repulsion between the embedded ions was overcome by the attractive potentials between atoms within the PEG chain (capillary forces), the structure was reasonably compact. It was hence expected to have a density close to the bulk PEG density, as did the folded, larger uncharged PEG 506-mer. We approximated the bulk density of PEG, ρ_{PEG}, with the temperature-dependent formula[48]

$$\rho_{PEG}(T) = 1.142 \exp[-7.09 \times 10^{-4}(T - 273)] \quad (14)$$

which results in a value of 1.115 g cm^{-3} for ρ_{PEG} at 304 K. This value is slightly lower than the value of 1.24 g cm^{-3} reported for ~12-kDa PEG ions by Saucy et al.,[8d] based on DMA measurements and the application of eqs 1a and 1b. Their inferred density, however, was based on a gas-molecule diameter of 4.5 Å, which is substantially larger than the more recent and consistent estimates of d_g = 3.1 Å near 300 K. Reanalysis of the data they provided with d_g = 3.1 Å leads to inferred densities in better agreement with the predictions of eq 14.

The average density of the PEG 254-mer and 506-mer structures found with MD was evaluated from knowledge of the ion mass and the average volume occupied by the PEG structure. Table 1 correspondingly lists the spherical equivalent radii for carbon, oxygen, and hydrogen atoms used in MM2 force fields for the simulation of PEG structures. With these atomic dimensions, the MD-determined PEG structures had densities of ~0.71 g cm^{-3}, well below the bulk value, and to match the bulk density of PEG, a 12% reduction in all linear dimensions (i.e., in both the effective atomic radii and the spacing between atoms within the structure) was required. The method noted above of rescaling candidate structure sizes is in agreement with the experimental evidence motivating this study, namely, when mobility measurements have been made on relatively compact particles, the mobility diameters inferred using eqs 1a and 1b are in excellent agreement with volume-equivalent diameters determined from the particle mass and bulk density.[8a,b] We further note that the rescaling factor was derived from only two candidate structures and applied to all structures of similar chemical composition; we do not advocate the use of a rescaling factor derived by forcing the predictions of a particular mobility calculation procedure to agree with experimental results.[16a,22]

Table 1. van der Waals Radii, Radii Input into the MM2 Simulations, Rescaled PEG Ion Radii, and Rescaled Tetraalkylammonium Ion Radii for Nitrogen, Carbon, Oxygen, and Hydrogen Atoms[a,b]

atom	vdW radius	MM2 radius	PEG ion radius	tetraalkyl ion radius
N	1.55	1.82	1.63	1.53
C	1.70	1.90	1.70	1.60
O	1.52	1.74	1.55	1.46
H	1−1.2	0.95−1.5	1.1−1.3	1.1−1.3

[a]All values are in angstroms. [b]Radii used in collision-cross-section calculation are in better agreement with the van der Waals radii than are the MM2 simulation input radii.

Although density values are not readily available for the tetraalkylammonium ions, with structures also generated by MM2 simulations, the resulting structures must also be rescaled to appropriate sizes. In this instance, we elected to reduce all linear dimensions of candidate structures by 19%, which was done in an attempt to bring the atomic radii of the hydrogen atoms (most of which are input in MM2 calculations at 1.5 Å) in line with their van der Waals radii (also included in Table 1). Hydrogen is the most abundant atom in tetraalkylammonium ions, hence our choice to rescale structures based on its size.

3.2. Test Case 1: Poly(ethylene glycol) Ions. The left side of Figure 3 shows a mass−mobility contour plot (where the abscissa is the inverse mobility, $1/Z_p$, in V s cm^{-2} and the ordinate is the mass-to-charge ratio, m_p/z, in Da) for electrospray-generated PEG ions in a wide molecular weight range. These results derive directly from the work of Larriba and Fernandez de la Mora,[17] who measured PEG ion mobilities at 304 K in air at atmospheric pressure by DMA. In the contour plot, signal intensity is displayed on a logarithmic scale colorimetrically, with black denoting the absence of signal above a certain threshold and color variation from blue to red denoting increasingly more intense ion signal. Apparent in this plot are distinct "curves" where PEG ion signal is detected, and each curve converges to an extremely intense band of signal at low $1/Z_p$ and m/z. As noted by Larriba and Fernandez de la Mora, each curve corresponds to ions with an identical excess charge state, and the excess charge states for several curves are labeled on the contour plot. The distinct kinks observed in each curve correspond to structural transitions in PEG ions, with the most massive ions of a given charge state highly globular and compact and the lowest-mass ions nearly linear. With all of these structural transitions identified and well-described, the structure of a specific PEG ion detected at a specified $1/Z_p$, m_p/z coordinate can be simulated and determined reliably. For comparison to mobility predictions, we specifically opted to examine PEG structures with 4+ excess positive charges with 254, 144, 115, 90, and 70 monomer units (labeled A−E, respectively, in Figure 3), but note that this choice is somewhat arbitrary, as any set of PEG ions chosen would lead to similar results. For guidance, a white dashed curve runs parallel to the 4+ curve in the contour plot. Valid mobility predictions for each of the examined ions should fall directly on the 4+ curve. Candidate PEG ion structures were generated by a procedure identical to that used to generate the 254-mer and 506-mer calibrant structures with reduction in linear dimensions. As for the PEG 506-mer and 254-mer, each examined ion converged to a characteristic morphology, with little structural variation once equilibrium was effectively established in the simulations. Representations of the obtained characteristic structures for each examined PEG ion are shown on the right side of Figure 3,

dx.doi.org/10.1021/jp312432z | J. Phys. Chem. A 2013, 117, 3887−3901

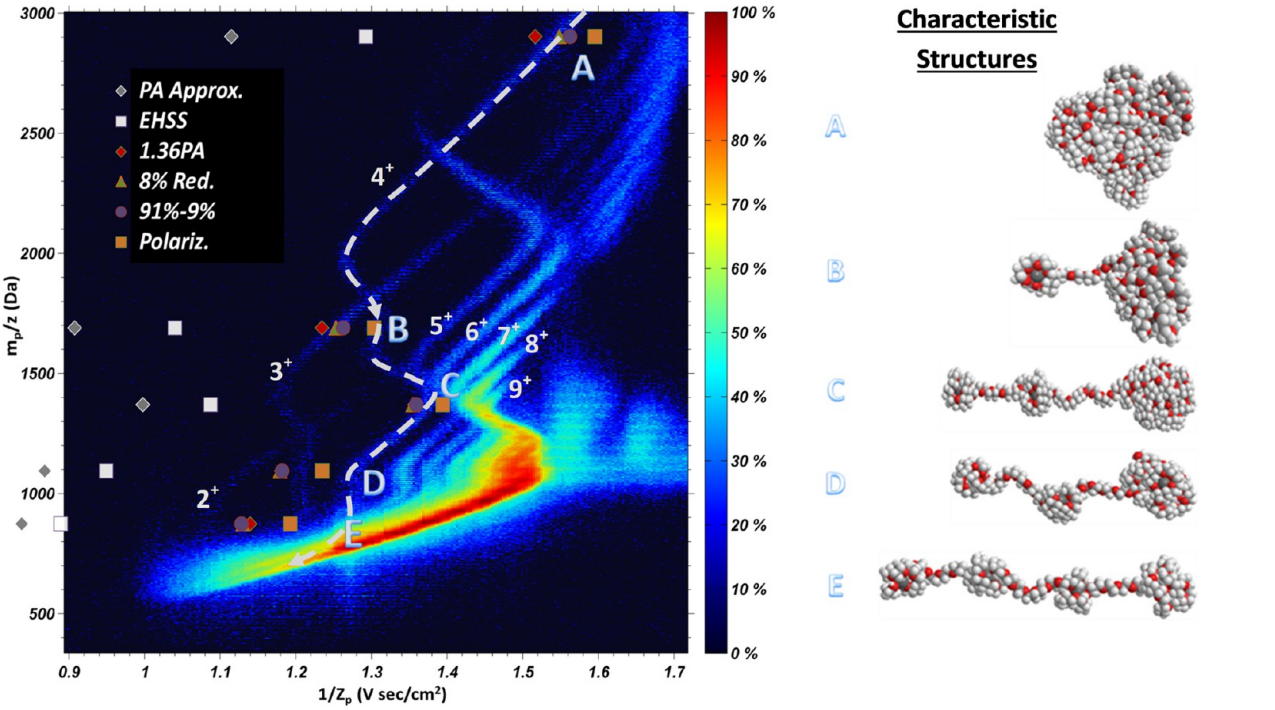

Figure 3. Mass−mobility contour plot for multiply charged poly(ethylene glycol) ions with the logarithm of the dimensionless signal intensity denoted by a colorimetric scale. For five examined 4+ ions (labeled A−E, with characteristic structures shown), mobility calculations were performed, and the resulting predicted m_p/z and inverse mobility values for different model predictions are overlaid on the contour plot. The measured m_p/z values and mobilities for 4+ ions are highlighted with a dashed white line. Abbreviations: PA Approx., projected area approximation; EHSS, elastic-hard-sphere scattering predictions with a finite-sized gas molecule; 1.36PA, mobility predictions with the collision cross section determined as 1.36 times the orientationally averaged projected area of each structure; 8% Red., DHSS calculations with an 8% reduction in the speed of the reemitted gas molecule; 91%−9%, DHSS calculations with a 91% diffuse-accommodating, 9% specular-elastic gas-molecule reemission model; Polariz., DHSS calculations with an 8% reduction in the speed of the reemitted gas molecule and consideration of the ion−induced dipole potential.

Table 2. Collision Cross Sections (Å^2) Determined from Six Different Calculation Procedures for 4+ Poly(ethylene glycol) Ions Composed of the Indicated Number of Monomers (N_{mon}) and Their Experimentally Inferred Collision Cross Sections in Air at Atmospheric Pressure and a Temperature of 304 K[a,b]

N_{mon}	PA approx	EHSS	1.36PA	91%−9% (DHSS)	8% red (DHSS)	polariz (DHSS)	expt	polar/expt
70	738.48	783.97	1004.33	994.36	995.73	1048.6	1090.99	0.961
90	764.61	836.13	1039.86	1040.80	1038.25	1083.76	1123.18	0.965
115	878.08	956.86	1194.19	1195.76	1191.77	1232.32	1225.05	1.006
144	798.41	915.034	1085.84	1110.33	1101.98	1146.12	1151.71	0.995
254	979.69	1135.79	1332.38	1372.73	1360.27	1400.19	1365.88	1.025

[a]Calculation methods invoking DHSS gas-molecule reemission models are indicated. [b]Abbreviations: PA approx, projected area approximation; EHSS, elastic-hard-sphere scattering predictions with a finite-sized gas molecule; 1.36PA, mobility predictions with the collision cross section determined as 1.36 times the orientationally averaged projected area of each structure; 91%−9%, DHSS calculations with a 91% diffuse-accommodating, 9% specular-elastic gas-molecule reemission model; 8% red, DHSS calculations with an 8% reduction in the speed of the reemitted gas molecule; Polariz, DHSS calculations with an 8% reduction in the speed of the reemitted gas molecule and consideration of the ion−induced dipole potential; expt, experimentally measured collision cross sections; polar/expt, dimensionless ratio of collision cross section calculated with the DHSS polarization model to the measured collision cross section.

where the variation from compact (254-mer) to completely stretched (70-mer) is clear.

For the test PEG structures, the predicted collision cross sections from all examined calculation methods and the experimentally inferred collision cross sections are listed in Table 2. We first determined the mobilities of test ions using procedures analogous to the traditional PA and EHSS methods. The resulting predicted $1/Z_p$, m_p/z coordinates for each ion are indicated with gray diamonds (PA method) and white squares (EHSS method) in the Figure 3 contour plot. It is readily apparent that neither of these methods gives rise to mobility predictions in line with the measurements, with both methods overestimating the mobility (underestimating the collision cross sections) of the test ions substantially. This underestimation is attributable to the failure of these methods to correctly model gas-molecule scattering and the momentum transferred from gas molecules to a particle/ion. The EHSS method does lead to predictions in closer agreement with experimental results than the PA method, as multiple scattering events in this method can lead to enhanced momentum transfer as compared to single, specular nonscattering events, which are assumed to be the sole form of momentum transfer in the PA method. However, multiple scattering events will not occur for all impinging gas molecules when a noninfinitesimal gas molecule is modeled,

dx.doi.org/10.1021/jp312432z | J. Phys. Chem. A 2013, 117, 3887−3901

and their occurrence is particularly rare in the elongated regions of the smaller examined PEG ions, which are only one to two atoms in thickness.

Collision-cross-section/mobility predictions invoking DHSS collision models, both the proposed fully diffuse-accommodating model with an 8% reduction in gas-molecule reemission speeds (the 8% reduction model) and the 91% diffuse-accommodating, 9% specular-elastic model (the 91%−9% model), are also listed in Table 2 and displayed in Figure 3. With the 8% reduction model, we performed both hard-sphere-only (green triangles) and polarization-included (orange squares) calculations, and for the 91%−9% model, we considered only hard-sphere atoms (violet circles). For ions with 115 monomer units and larger, all three of these calculation procedures gave rise to predictions in excellent agreement with experimental measurements (within 2−3% of the average collision cross sections), with the 91%−9% model predicting only slightly lower mobilities than the 8% reduction model. For the 90-mer and 70-mer ions, the calculation procedures considering only hard-sphere atoms slightly overestimated the measured mobilities, indicating that the long-range polarization force influences momentum transfer to these structures. Indeed, predictions incorporating the polarization potential were found to be in better agreement with measurements for these ions (within 4% of the average collision cross sections).

Clearly, diffuse scattering models are needed to reliably predict mobilities for PEG ions in air from structural models with reasonably sized atoms and gas molecules. However, we note that, although the PA method predictions alone strongly disagree with measurements, the degree of disagreement between predicted collision cross sections is a constant of ~36% for large structures; that is, PEG ion-mobility measurements suggest $\Omega = \xi PA$, where PA is the orientationally average projected area of the ion−gas-molecule complex[24] and, as found with the Stokes−Millikan equation,[13] $\xi = 1.36$. Predictions for PEG ions calculating the collision cross section in this way are also shown in the Figure 3 contour plot (red diamonds), and their agreement with both DHSS predictions and measurements suggests that $\Omega = \xi PA$ might be a reasonable approximation not only for spherical structures (eq 1b) but for all particles in the absence of any long-range potential.

3.3. Test Case 2: Tetraalkylammonium Ions. The tetramethylammonium (TMA^+), tetrapropylammonium (TPA^+), tetrabutylammonium (TBA^+), tetraheptylammonium (THA^+), tetradecylammonium (TDA^+), and tetradodecylammonium ($TDDA^+$) cations, also generated by electrospray ionization, have mobilities measured in air and atmospheric pressure at 293 K by Ude and Fernandez de la Mora[18] that agree well with other independent measurements of their mobilities under similar conditions.[26b,45b] For comparison, candidate structures of these ions were generated with MD, enabling mobility prediction and comparison to the published results. However, unlike PEG ions, tetraalkylammonium ions do not adopt specific structures at equilibrium; rather, MD simulations reveal that these ions, particularly those with longer alkyl chains, can probe a broad spectrum of conformations, ranging from collapsed to highly branched. Therefore, mobility predictions were performed using 3−20 conformers for each tetraalkylhalide ion, selected randomly after simulations had been run for 20 ps. For comparison to measurements, the predicted mobilities for each tetraalkylammonium ion were taken as the average of the mobilities of all examined conformers.

Before directly comparing measured mobilities to predictions, we further examine the finding with PEG ions that $\Omega = \xi PA$ in the absence of polarization potential influences. Figure 4

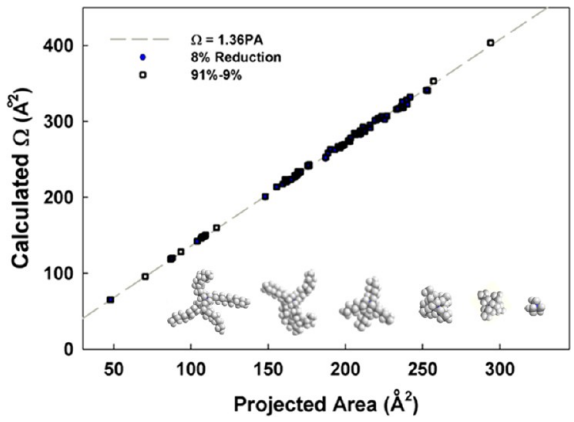

Figure 4. Comparison between the orientationally averaged projected area of 77 MD-generated tetraalkylammonium structures and the collision cross sections for these structures calculated using DHSS methods. The dashed line denotes the approximation that the collision cross section is 1.36 times the orientationally averaged projected area.

compares the collision cross sections determined with the 8% reduction and the 91%−9% models to the orientationally averaged projected areas of the gas-molecule−ion complexes for 77 distinct tetraalkylammonium cation candidate structures. In addition to the two diffuse scattering methods again converging to near-identical results, the Ω versus PA values for all structures collapse to a single, highly linear curve with a slope of $\xi = 1.36$, further supporting use of the approximation $\Omega = \xi PA$.

However, because of their small size, many tetraalkylammonium cations have collision cross sections that are strongly influenced by gas-molecule polarization. This is clearly evident in Figure 5, where example gas-molecule trajectories near a THA^+ cation (left side) and a TMA^+ cation (right side) are displayed. In both cases, the gas-molecule incoming speed into the control volume is the mean thermal speed at 293 K (for air). The apparent curvilinearity of the trajectories in both cases is indicative of the polarization potential between the central charged nitrogen atom in each ion and the oncoming gas molecule. Thus, although Ω calculated by hard-sphere methods agrees well with 1.36PA, this will not be the case when the polarization potentials are considered, nor are experimental measurements expected to agree with hard-sphere predictions for tetralkylammonium ions. Figure 6 shows a plot of the predicted inverse mobilities of tetraalkylammonium ions as a function of their corresponding reported inverse mobility values from experiments. Predictions were performed matching the gas pressure and temperature to experiments with the EHSS method with polarization, the 8% reduction hard-sphere diffuse scattering method (squares) without polarization, and the 8% reduction diffuse scattering method with polarization. For guidance, a dashed 1:1 line is also plotted. As for PEG ions, the EHSS method leads to overestimation of the mobility (underestimation of the inverse mobility) as compared to measurements. Again, this follows directly from the assumption of purely specular scattering. Conversely, DHSS calculations

dx.doi.org/10.1021/jp312432z | J. Phys. Chem. A 2013, 117, 3887−3901

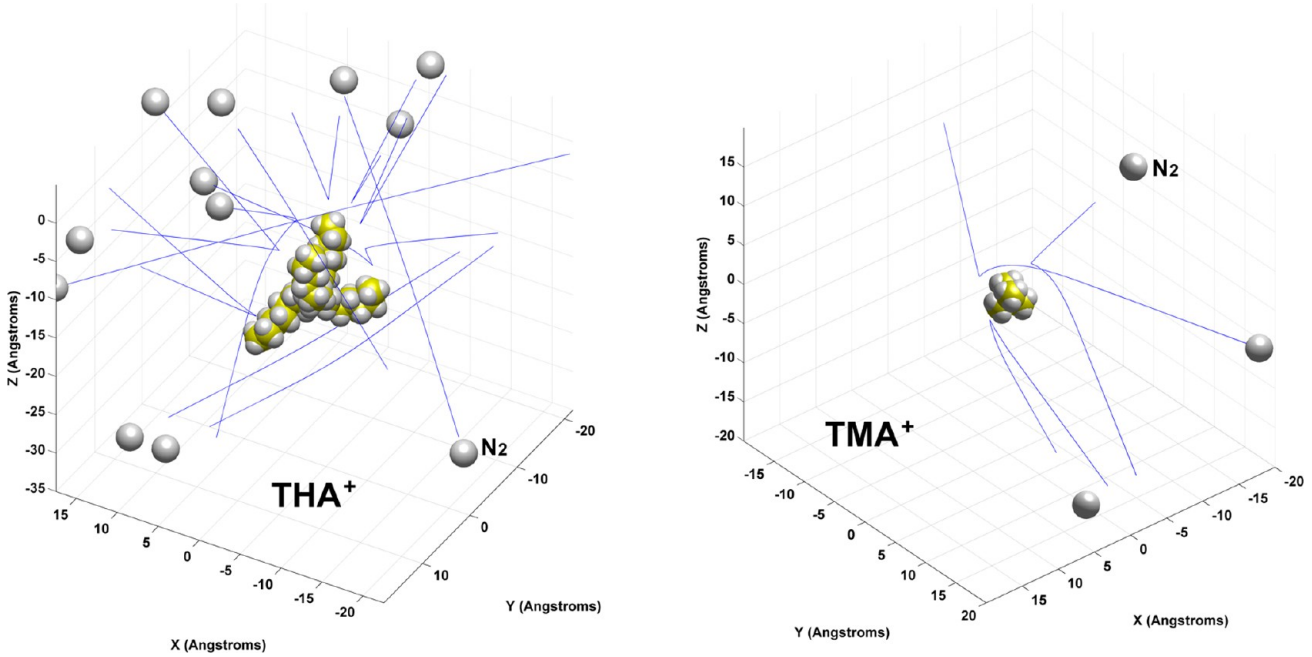

Figure 5. Pathlines portraying nitrogen gas-molecule trajectories near one tetraheptylammonium$^+$ (right side) and one tetramethylammonium$^+$ (left side) cation, considering the influence of the ion−induced dipole potential at 293 K.

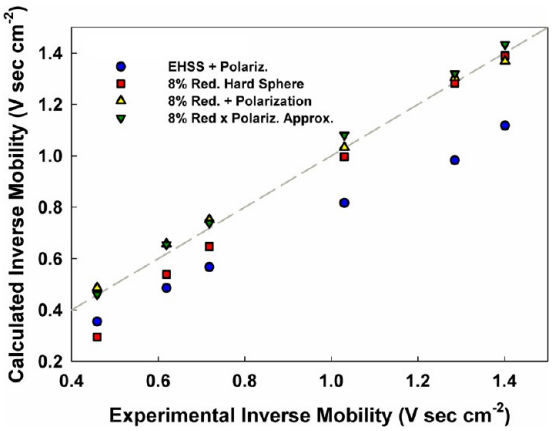

Figure 6. Predicted inverse mobilities for tetraalkylammonium ions as a function of experimentally measured inverse mobilities for the same ions at 293 K and atmospheric pressure. The dashed gray line denotes a 1:1 ratio. Abbreviations: EHSS + Polariz., EHSS calculations considering the ion−induced dipole potential between gas molecule and ion; 8% Red. Hard Sphere, DHSS calculations with an 8% reduction in the speed of the reemitted gas molecule, without potential interactions; 8% Red. + Polariz., DHSS calculations with an 8% reduction in the speed of the reemitted gas molecule considering the ion−induced dipole potential; 8% Red. x Polariz. Approx., DHSS calculations with an 8% reduction in the speed of the reemitted gas molecule and the collision cross section determined by multiplying the calculation result by an algebraic approximation for the influence of polarization (eq 15a).

without considering polarization are in excellent agreement with measurements of the larger tetraalkylammonium ions, but they overestimate the mobilities of the smaller ions. This underestimation is clearly brought about by the neglect of polarization, and the disagreement between measurements and hard-sphere non-specular scattering methods is nearly completely remedied by incorporating polarization potentials into calculations (measurements and predictions are within 5% of one another in all cases). Furthermore, that the influence of polarization is correctly taken into account by calculations strongly supports the candidate structure rescaling procedure employed; without rescaling, the influence of polarization would be mitigated, and no employed scattering law would allow for calculation predictions to match experimentally measured collision cross sections.

3.4. Approximating the Collision Cross Section with Projected Area. Comparison of both the 8% reduction and 91%−9% scattering methods to measurements reveals that some form of diffuse scattering must be considered to correctly predict mobilities in diatomic gases with reasonably sized candidate structures. However, scattering calculations can become time-consuming and cumbersome, particularly when applied to structures composed of $>10^4$ atoms.[39a,49] It is therefore highly desirable to relate the orientationally averaged projected area, PA, of an ion−gas-molecule complex to the collision cross section, as this parameter can be calculated much more simply, even when nonspherical gas molecules are considered.[50] In the absence of polarization, we find overwhelmingly that the approximation $\Omega = \xi$PA holds valid. It is hence reasonable to also suggest that an equation of the following form will hold valid for all gas conditions

$$\Omega = L\xi\mathrm{PA} \tag{15a}$$

where L is a correction factor for polarization. As shown elsewhere, in good agreement with calculations reported by Mason and McDaniel,[2] L can be approximated for a sphere by the equations

$$\mathcal{L} \approx \left[1 + \varphi_e\left(\frac{1}{3.1} + \frac{1}{\xi}\left(\frac{1}{16} + \frac{4}{33}\varphi_e\right)\right)\right] \qquad \text{if } \varphi_e \leq 1 \tag{15b}$$

dx.doi.org/10.1021/jp312432z | J. Phys. Chem. A 2013, 117, 3887−3901

$$\mathcal{L} \simeq \left[1 + \varphi_e\left(\frac{1}{4} - \frac{2.3}{1000}\varphi_e + \frac{1}{\xi}\left(\frac{9}{56} - \frac{6.8}{1000}\varphi_e\right)\right)\right] \quad \text{if } \varphi_e > 1 \tag{15c}$$

where $\varphi_e = U_{pol}[(d_p + d_g)/2]/kT$ denotes the polarization potential evaluated at a distance of $(d_p + d_g)/2$. In the case of nonspherical particles, $(d_p + d_g)/2$ can be approximated by the value $(PA/\pi)^{1/2}$. Equations 15b and 15c are based on the separate analyses of momentum transfer due to grazing collisions (terms with the factor $1/\xi$) and due to momentum transfer by direct impinging collisions on a sphere of equivalent radius; the coefficients were not derived from experimental data. The value where φ_e becomes unity corresponds at T = 300 K to a particle diameter of 6.3 Å; experimentally, only the radius of the TMA^+ cation is below this threshold. As a test of this approximation, Figure 6 also shows the inverse mobility predicted for tetraalkylammonium ions based on eqs 1a, 15a , 15b , and 15c using the average projected area from all sampled structures for each ion to compute results with eqs 15b and 15c, as a function of the measured inverse mobility. Overall, the agreement between the approximation predictions and the measured mobilities is excellent, and although it is not theoretically confirmed that the collision cross section can be expressed as the product of a geometric component (PA), a momentum scattering coefficient (ξ), and a potential interaction correction (L), this might be a reasonable method of approximating the collision cross section for charged particles in diatomic gases.

Finally, in regards to eq 15a, we remark that it has been customary to treat the PA approximation, hard-sphere scattering calculations, and trajectory calculations considering potentials as three separate modes of mobility prediction.[49,51] Doing so, however, reveals a misunderstanding in the reason charged particles moving in a background gas have a measurable ion mobility. Ion mobility is a measurable parameter not because it is an intrinsic property of a particle or a particle−gas-molecule combination; rather, it is a measure of the drag force experienced by a particle when low-speed relative motion exists between the particle and the surrounding background gas. This drag force is clearly influenced by the three factors input into eq 15a: the geometry of the particle, the amount of momentum transferred to a particle by each impinging gas molecule, and the enhancement in collisions and onset of grazing collisions brought about by potentials. PA approximations consider only the first of these effects and therefore need to be augmented by momentum scattering coefficients and potential interaction correction factors. Similarly, hard-sphere scattering approaches should be augmented by potential interaction correction factors. Such corrections should be implemented in a manner that mobility predictions with PA approximations, hard-sphere scattering models, and trajectory methods are in reasonable agreement with one another, as is seen here for both PEG and tetraalkylammonium test ions. Drastically different predictions deriving from these methods arise only when correction factors have not been correctly applied in PA and hard-sphere scattering calculation methods or the size of the particle and gas-molecule pair under examination is not treated equally in all three prediction methods.

4. CONCLUSIONS

Momentum-transfer/ion-mobility calculations were performed using all-atom models of particles and non-specular, inelastic gas-molecule scattering from particle surfaces. These scattering models are semiempirical, designed to mimic energy transfer between translational, rotational, and vibrational energies during gas-molecule−particle collisions, and the collision rules are designed such that predictions are in line with the Stokes−Millikan equation. The mobilities of particles predicted with this calculation procedure agree well with experimental measurements in air of multiply charged PEG and singly charged tetraheptylammonium ions. Preexisting mobility calculation procedures, the PA approximation and EHSS method, lead to predicted mobilities that are substantially higher than measurements and do not agree with the predictions of the Stokes−Millikan equation. For the highest-mobility ions examined, it was found that one must consider not only non-specular inelastic scattering at particle surfaces, but also the influence of the ion−induced dipole potential for sufficiently polarizable gas molecules, such as N_2 and O_2.

Based on the developed calculation procedure and comparison to experimental measurements, we conclude that, although non-specular, inelastic scattering models are clearly needed to correctly predict ion mobilities in diatomic gases, the precise form of the gas-molecule scattering law is not yet clear, and a number of different scattering laws can be developed that lead to predictions in good agreement with experimental results. Future work will be necessary to better understand gas-molecule scattering from particle surfaces and to develop procedures for correctly modeling energy transfer during this process. Furthermore, when using conventional molecular dynamics approaches to determine candidate particle structures for mobility calculations, a mechanism to resize the candidate structures such that their densities are in line with known values is needed. Without rescaling, the fact that non-specular, inelastic scattering is needed to predict mobilities is less evident. Finally, although not theoretically rigorous, calculation and experimental results suggest that, in diatomic, polarizable gases, the collision cross section of any particle/ion can be approximated by the relation $\Omega = L\xi PA$, where L is a correction (enhancement) factor to account for the influence of the ion−induced dipole potential, ξ is a momentum scattering factor (1.36 based on measurements), and PA is the orientationally averaged projected area of the particle−gas-molecule complex. Further testing of this approximation should be performed to determine whether it can be used reliably in a wide variety of circumstances for mobility prediction.

■ ASSOCIATED CONTENT

Supporting Information

A video of the simulated folding of a 506-mer PEG chain in vacuo and derivation of the momentum scattering coefficient for the 8% reduction scattering rule. This material is available free of charge via the Internet at http://pubs.acs.org.

■ AUTHOR INFORMATION

Corresponding Author

*E-mail: clarriba@umn.edu.

Notes

The authors declare no competing financial interest.

■ ACKNOWLEDGMENTS

This work was supported by NSF Grant CHE-1011810. C.L. also acknowledges support from the Ramon Areces Foundation. Both authors thank Prof. Juan Fernandez de la Mora for his careful instruction on gas-phase mobility analysis.

■ REFERENCES

(1) (a) Fernandez de la Mora, J.; de Juan, L.; Eichler, T.; Rosell, J. Differential Mobility Analysis of Molecular Ions and Nanometer Particles. *TrAC, Trends Anal. Chem.* **1998**, *17* (6), 328−339. (b) Bohrer, B. C.; Merenbloom, S. I.; Koeniger, S. L.; Hilderbrand, A. E.; Clemmer, D. E. Biomolecule Analysis by Ion Mobility Spectrometry. *Annu. Rev. Anal. Chem.* **2008**, *1*, 293−327.

(2) Mason, E. A.; McDaniel, E. W. *Transport Properties of Ions in Gases*; Wiley: New York, 1988.

(3) Jiang, J.; Zhao, J.; Chen, M.; Eisele, F.; Scheckman, J. H.; Williams, B. J.; Kuang, C.; McMurry, P. H. First Measurements of Neutral Atmospheric Cluster and 1−2 nm Particle Number Size Distributions during Nucleation Events. *Aerosol Sci. Technol.* **2011**, *45*, ii−v.

(4) Ruotolo, B. T.; Benesch, J. L. P.; Sandercock, A. M.; Hyung, S. J.; Robinson, C. V. Ion Mobility−Mass Spectrometry Analysis of Large Protein Complexes. *Nat. Protoc.* **2008**, *3* (7), 1139−1152.

(5) Epstein, P. S. On the Resistance Experienced by Spheres in Their Motion through Gases. *Phys. Rev.* **1924**, *23*, 710−733.

(6) Fernandez de la Mora, J.; de Juan, L.; Liedtke, K.; Schmidt-Ott, A. Mass and Size Determination of Nanometer Particles by Means of Mobility Analysis and Focused Impaction. *J. Aerosol Sci.* **2003**, *34* (1), 79−98.

(7) Hogan, C. J.; Fernandez de la Mora, J. Ion Mobility Measurements of Non-Denatured 12−150 kDa Proteins and Protein Multimers by Tandem Differential Mobility Analysis−Mass Spectrometry (DMA-MS). *J. Am. Soc. Mass Spectrom.* **2011**, *22*, 158−172.

(8) (a) Larriba, C.; Hogan, C. J.; Attoui, M.; Borrajo, R.; Fernandez-Garcia, J.; Fernandez de la Mora, J. The Mobility−Volume Relationship below 3.0 nm Examined by Tandem Mobility−Mass Measurement. *Aerosol Sci. Technol.* **2011**, *45*, 453−467. (b) Ku, B. K.; Fernandez de la Mora, J. Relation between Electrical Mobility, Mass, and Size for Nanodrops 1−6.5 nm in Diameter in Air. *Aerosol Sci. Technol.* **2009**, *43* (3), 241−249. (c) Ude, S.; Fernandez de la Mora, J.; Alexander, J. N.; Saucy, D. A. Aerosol Size Standards in the Nanometer Size Range II. Narrow Size Distributions of Polystyrene 3−11 nm in Diameter. *J. Colloid Interface Sci.* **2006**, *293* (2), 384−393. (d) Saucy, D. A.; Ude, S.; Lenggoro, I. W.; Fernandez de la Mora, J. Mass Analysis of Water-Soluble Polymers by Mobility Measurement of Charge-Reduced Ions Generated by Electrosprays. *Anal. Chem.* **2004**, *76* (4), 1045−1053. (e) Ku, B. K.; Fernandez de la Mora, J.; Saucy, D. A.; Alexander, J. N. Mass Distribution Measurement of Water-Insoluble Polymers by Charge-Reduced Electrospray Mobility Analysis. *Anal. Chem.* **2004**, *76* (3), 814−822. (f) Borysik, A. J.; Robinson, C. V. The 'Sticky Business' of Cleaning Gas-Phase Membrane Proteins: A Detergent Oriented Perspective. *Phys. Chem. Chem. Phys.* **2012**, *14* (42), 14439−14449.

(9) (a) Kim, J. H.; Mulholland, G. W.; Kukuck, S. R.; Pui, D. Y. H. Slip Correction Measurements of Certified PSL Nanoparticles Using a Nanometer Differential Mobility Analyzer (Nano-DMA) for Knudsen Number from 0.5 to 83. *J. Res. Natl. Inst. Stand. Technol.* **2005**, *110* (1), 31−54. (b) Hogan, C. J.; Kettleson, E. M.; Ramaswami, B.; Chen, D. R.; Biswas, P. Charge Reduced Electrospray Size Spectrometry of Mega- and Gigadalton Complexes: Whole Viruses and Virus Fragments. *Anal. Chem.* **2006**, *78* (3), 844−852.

(10) Cunningham, E. On the Velocity of Steady Fall of Spherical Particles through Fluid Medium. *Proc. R. Soc. London A* **1910**, *83* (563), 357−365.

(11) Millikan, R. A. A New Modification of the Cloud Method of Determining the Elementary Electrical Charge and the Most Probable Value of That Charge. *Philos. Mag.* **1910**, *19*, 209−228.

(12) (a) Millikan, R. A. The General Law of Fall of a Small Spherical Body through a Gas, and Its Bearing upon the Nature of Molecular Reflection from Surfaces. *Phys. Rev.* **1923**, *22*, 1−23. (b) Eglin, J. M. The Coefficients of Viscosity and Slip of Carbon Dioxide by the Oil Drop Method and the Law of Motion of an Oil Drop in Carbon Dioxide, Oxygen, and Helium, at Low Pressures. *Phys. Rev.* **1923**, *22*, 161−170.

(13) Davies, C. N. Definitive Equations for the Fluid Resistance of Spheres. *Proc. Phys. Soc.* **1945**, *57*, 259−270.

(14) (a) Rader, D. G. Momentum Slip Correction Factor for Small Particles in Nine Common Gases. *J. Aerosol Sci.* **1990**, *21*, 161−168. (b) Allen, M. D.; Raabe, O. G. Slip Correction Measurements of Spherical Solid Aerosol Particles in an Improved Millikan Apparatus. *Aerosol Sci. Technol.* **1985**, *4*, 269−286. (c) Allen, M. D.; Raabe, O. G. Re-Evaluation of Millikan's Oil Drop Data for the Motion of Small Particles in Air. *J. Aerosol Sci.* **1982**, *13*, 537. (d) Jung, H.; Mulholland, G. W.; Pui, D. Y. H.; Kim, J. H. Re-Evaluation of the Slip Correction Parameter of Certified PSL Spheres Using a Nanometer Differential Mobility Analyzer (NDMA). *J. Aerosol Sci.* **2012**, *51*, 24−34.

(15) (a) Shvartsburg, A. A.; Mashkevich, S. V.; Baker, E. S.; Smith, R. D. Optimization of Algorithms for Ion Mobility Calculations. *J. Phys. Chem. A* **2007**, *111* (10), 2002−2010. (b) Pease, L. F.; Elliott, J. T.; Tsai, D. H.; Zachariah, M. R.; Tarlov, M. J. Determination of Protein Aggregation with Differential Mobility Analysis: Application to IgG Antibody. *Biotechnol. Bioeng.* **2008**, *101* (6), 1214−1222.

(16) (a) Shvartsburg, A. A.; Jarrold, M. F. An Exact Hard-Spheres Scattering Model for the Mobilities of Polyatomic Ions. *Chem. Phys. Lett.* **1996**, *261* (1−2), 86−91. (b) Kinnear, B. S.; Kaleta, D. T.; Kohtani, M.; Hudgins, R. R.; Jarrold, M. F. Conformations of Unsolvated Valine-Based Peptides. *J. Am. Chem. Soc.* **2000**, *122* (38), 9243−9256. (c) Shvartsburg, A. A.; Liu, B.; Jarrold, M. F.; Ho, K. M. Modeling Ionic Mobilities by Scattering on Electronic Density Isosurfaces: Application to Silicon Cluster Anions. *J. Chem. Phys.* **2000**, *112* (10), 4517−4526. (d) Hudgins, R. R.; Imai, M.; Jarrold, M. F.; Dugourd, P. High-Resolution Ion Mobility Measurements for Silicon Cluster Anions and Cations. *J. Chem. Phys.* **1999**, *111* (17), 7865−7870.

(17) Larriba, C.; Fernandez de la Mora, J. The Gas Phase Structure of Coulombically Stretched Polyethylene Glycol Ions. *J. Phys. Chem. B* **2012**, *116*, 593−598.

(18) Ude, S.; Fernandez de la Mora, J. Molecular Monodisperse Mobility and Mass Standards from Electrosprays of Tetra-Alkyl Ammonium Halides. *J. Aerosol Sci.* **2005**, *36* (10), 1224−1237.

(19) Larriba, C.; Hogan, C. J., manuscript submitted.

(20) Bleiholder, C.; Wyttenbach, T.; Bowers, M. T. A Novel Projection Approximation Algorithm for the Fast and Accurate Computation of Molecular Collision Cross Sections (I). Method. *Int. J. Mass Spectrom.* **2011**, *308* (1), 1−10.

(21) Wyttenbach, T.; vonHelden, G.; Batka, J. J.; Carlat, D.; Bowers, M. T. Effect of the Long-Range Potential on Ion Mobility Measurements. *J. Am. Soc. Mass Spectrom.* **1997**, *8* (3), 275−282.

(22) Mesleh, M. F.; Hunter, J. M.; Shvartsburg, A. A.; Schatz, G. C.; Jarrold, M. F. Structural Information from Ion Mobility Measurements: Effects of the Long-Range Potential. *J. Phys. Chem.* **1996**, *100* (40), 16082−16086.

(23) Garcia-Ybarra, P.; Rosner, D. E. Thermophoretic Properties of Nonspherical Particles and Large Molecules. *AIChE J.* **1989**, *35*, 139−147.

(24) Zhang, C.; Thajudeen, T.; Larriba, C.; Schwartzentruber, T. E.; Hogan, C. J. Determination of the Scalar Friction Factor for Non-Spherical Particles and Aggregates across the Entire Knudsen Number Range by Direct Simulation Monte Carlo (DSMC). *Aerosol Sci. Technol.* **2012**, *46*, 1065−1078.

(25) Happel, J.; Brenner, H. *Low Reynolds Number Hydrodynamics*; Martinus Nijhoff Publishers: The Hague, The Netherlands, 1983.

(26) (a) Kim, H.; Kim, H. I.; Johnson, P. V.; Beegle, L. W.; Beauchamp, J. L.; Goddard, W. A.; Kanik, I. Experimental and Theoretical Investigation into the Correlation between Mass and Ion Mobility for Choline and Other Ammonium Cations in N_2. *Anal.*

Chem. **2008**, *80* (6), 1928−1936. (b) Campuzano, I.; Bush, M. F.; Robinson, C. V.; Beaumont, C.; Richardson, K.; Kim, H.; Kim, H. I. Structural Characterization of Drug-Like Compounds by Ion Mobility Mass Spectrometry: Comparison of Theoretical and Experimentally Derived Nitrogen Collision Cross Sections. *Anal. Chem.* **2012**, *84* (2), 1026−1033.

(27) (a) Niwa, M.; Yamazaki, K.; Murakami, Y. Separation of Oxygen and Nitrogen Due to the Controlled Pore-Opening Size of Chemically Vapor Deposited Zeolite A. *Ind. Eng. Chem. Res.* **1991**, *30* (1), 38−42. (b) Tammet, H. The Function-Updated Millikan Model: A Tool for Nanometer Particle Size-Mobility Conversions. *Aerosol Sci. Technol.* **2012**, *46*, i−iv.

(28) Kim, H. I.; Kim, H.; Pang, E. S.; Ryu, E. K.; Beegle, L. W.; Loo, J. A.; Goddard, W. A.; Kanik, I. Structural Characterization of Unsaturated Phosphatidylcholines Using Traveling Wave Ion Mobility Spectrometry. *Anal. Chem.* **2009**, *81* (20), 8289−8297.

(29) Fernandez de la Mora, J. Free-Molecule Mobility of Polyhedra and Other Convex Hard Bodies. *J. Aerosol Sci.* **2002**, *33* (3), 477−489.

(30) Vincenti, W. G.; Kruger, C. H. *Introduction to Physical Gas Dynamics*; Krieger: Huntington, NY, 1975.

(31) Mackowski, D. W. Monte Carlo Simulation of Hydrodynamic Drag and Thermophoresis of Fractal Aggregates of Spheres in the Free-Molecule Flow Regime. *J. Aerosol Sci.* **2006**, *37*, 242−259.

(32) Chan, P.; Dahneke, B. Free-Molecule Drag on Straight Chains of Uniform Sphere. *J. Appl. Phys.* **1981**, *52*, 3106−3110.

(33) Lanvegin, P. Une Formule Fondamentale De Theorie Cinetique. *Ann. Chim. Phys.* **1905**, *8*, 266−279.

(34) Lenard, P.; Weick, W.; Mayer, H. F. Über Elektrizitätsleitung durch freie Elektronen und Träger. III: Wanderungsgeschwindigkeit kraftgetriebener Partikel in reibenden Medien. *Ann. Phys.* **1920**, *366*, 665−741.

(35) (a) Friedlander, S. K. *Smoke, Dust, and Haze*; Oxford University Press: New York, 2000; (b) Tammet, H. Size and Mobility of Nanometer Particles, Clusters and Ions. *J. Aerosol Sci.* **1995**, *26* (3), 459−475.

(36) (a) Li, Z.; Wang, H. Drag Force, Diffusion Coefficient, and Electric Mobility of Small Particles. II. Application. *Phys. Rev. E* **2003**, *68*, 061207. (b) Li, Z.; Wang, H. Drag Force, Diffusion Coefficient, and Electric Mobility of Small Particles. I. Theory Applicable to the Free-Molecule Regime. *Phys. Rev. E* **2003**, *68*, 061206. (c) Li, Z. G.; Wang, H. Gas−Nanoparticle Scattering: A Molecular View of Momentum Accommodation Function. *Phys. Rev. Lett.* **2005**, *95* (1), 014502.

(37) (a) Valentini, P.; Schwartzentruber, T. E.; Cozmuta, I. Reaxff Grand Canonical Monte Carlo Simulation of Adsorption and Dissociation of Oxygen on Platinum(111). *Surf. Sci.* **2011**, *605* (23−24), 1941−1950. (b) Valentini, P.; Schwartzentruber, T. E.; Cozmuta, I. Molecular Dynamics Simulation of O_2 Sticking on Pt(111) Using the ab Initio Based ReaxFF Reactive Force Field. *J. Chem. Phys.* **2010**, *133*, 8.

(38) (a) Hill, H. H.; Hill, C. H.; Asbury, G. R.; Wu, C.; Matz, L. M.; Ichiye, T. Charge Location on Gas Phase Peptides. *Int. J. Mass Spectrom.* **2002**, *219* (1), 23−37. (b) Steiner, W. E.; English, W. A.; Hill, H. H. Ion−Neutral Potential Models in Atmospheric Pressure Ion Mobility Time-of-Flight Mass Spectrometry IM(tof)MS. *J. Phys. Chem. A* **2006**, *110* (5), 1836−1844. (c) Beegle, L. W.; Kanik, I.; Matz, L.; Hill, H. H. Effects of Drift-Gas Polarizability on Glycine Peptides in Ion Mobility Spectrometry. *Int. J. Mass Spectrom.* **2002**, *216* (3), 257−268.

(39) (a) Hogan, C. J.; Ruotolo, B. T.; Robinson, C. V.; Fernandez de la Mora, J. Tandem Differential Mobility Analysis-Mass Spectrometry Reveals Partial Collapse of the GroEL Complex. *J. Phys. Chem. B* **2011**, *115*, 3614−4621. (b) Fernandez de la Mora, J. Why Do GroEL Ions Exhibit Two Gas Phase Conformers? *J. Am. Soc. Mass Spectrom.* **2012**, *23*, 2115−2121. (c) Fernandez de la Mora, J.; Borrajo, R.; Zurita-Gotor, M. Capillary and Coulombic Effects on the Gas Phase Structure of Electrosprayed Concanavalin A Ions and Its Clusters C_n^{+z} (n = 1−6). *J. Phys. Chem. B* **2012**, *116*, 9882−9898.

(40) Allen, M. P.; Tildesley, D. J. *Computer Simulation of Liquids*; Oxford Science Publications: Oxford, U.K., 1987.

(41) (a) Rosell-Llompart, J.; Loscertales, I. G.; Bingham, D.; Fernandez de la Mora, J. Sizing Nanoparticles and Ions with a Short Differential Mobility Analyzer. *J. Aerosol Sci.* **1996**, *27* (5), 695−719. (b) Hogan, C. J.; Fernandez de la Mora, J. Tandem Ion Mobility-Mass Spectrometry (IMS-MS) Study of Ion Evaporation from Ionic Liquid-Acetonitrile Nanodrops. *Phys. Chem. Chem. Phys.* **2009**, *11* (36), 8079−8090. (c) Rus, J.; Moro, D.; Sillero, J. A.; Royuela, J.; Casado, A.; Estevez-Molinero, F.; Fernandez de la Mora, J. IMS−MS Studies Based on Coupling a Differential Mobility Analyzer (DMA) to Commercial API−MS Systems. *Int. J. Mass Spectrom.* **2010**, *298*, 30−40.

(42) Maisser, A.; Premnath, V.; Ghosh, A.; Nguyen, T. A.; Attoui, M.; Hogan, C. J. Determination of Gas Phase Protein Ion Densities via Ion Mobility Analysis with Charge Reduction. *Phys. Chem. Chem. Phys.* **2011**, *13* (48), 21630−21641.

(43) (a) Wyttenbach, T.; von Helden, G.; Bowers, M. T. Conformations of Alkali Ion Cationized Polyethers in the Gas Phase: Polyethylene Glycol and Bis[(benzo-15-crown-5)-15-ylmethyl] Pimelate. *Int. J. Mass Spectrom.* **1997**, *165*, 377−390. (b) Ude, S.; Fernandez de la Mora, J.; Thomson, B. A. Charge-Induced Unfolding of Multiply Charged Polyethylene Glycol Ions. *J. Am. Chem. Soc.* **2004**, *126* (38), 12184−12190. (c) Trimpin, S.; Clemmer, D. E. Ion Mobility Spectrometry/Mass Spectrometry Snapshots for Assessing the Molecular Compositions of Complex Polymeric Systems. *Anal. Chem.* **2008**, *80* (23), 9073−9083.

(44) Consta, S.; Chung, J. K. Charge-Induced Conformational Changes of PEG-$(Na^+)_n$ in a Vacuum and Aqueous Nanodroplets. *J. Phys. Chem. B* **2011**, *115* (35), 10447−10455.

(45) (a) Ehn, M.; Junninen, H.; Schobesberger, S.; Manninen, H. E.; Franchin, A.; Sipila, M.; Petaja, T.; Kerminen, V. M.; Tammet, H.; Mirme, A.; Mirme, S.; Horrak, U.; Kulmala, M.; Worsnop, D. R. An Instrumental Comparison of Mobility and Mass Measurements of Atmospheric Small Ions. *Aerosol Sci. Technol.* **2011**, *45* (4), 522−532. (b) Jiang, J. K.; Attoui, M.; Heim, M.; Brunelli, N. A.; McMurry, P. H.; Kasper, G.; Flagan, R. C.; Giapis, K.; Mouret, G. Transfer Functions and Penetrations of Five Differential Mobility Analyzers for Sub-2 nm Particle Classification. *Aerosol Sci. Technol.* **2011**, *45* (4), 480−492.

(46) Allinger, N. L. Conformational Analysis. 130. MM2. Hydrocarbon Force Field Utilizing V1 and V2 Torsional Terms. *J. Am. Chem. Soc.* **1977**, *99* (25), 8127−8134.

(47) Stubbs, J. M.; Potoff, J. J.; Siepmann, J. I. Transferable Potentials for Phase Equilibria. 6. United-Atom Description for Ethers, Glycols, Ketones, and Aldehydes. *J. Phys. Chem. B* **2004**, *108* (45), 17596−17605.

(48) Jain, R. K.; Simha, R. Equation of State of Semicrystalline and Crystalline Polymers. *J. Polym. Sci. B: Polym. Phys.* **1979**, *17* (11), 1929−1946.

(49) van Duijn, E.; Barendregt, A.; Synowsky, S.; Versluis, C.; Heck, A. J. R. Chaperonin Complexes Monitored by Ion Mobility Mass Spectrometry. *J. Am. Chem. Soc.* **2009**, *131* (4), 1452−1459.

(50) Thajudeen, T.; Gopalakrishnan, R.; Hogan, C. J. The Collision Rate of Non-Spherical Particles and Aggregates for All Diffusive Knudsen Numbers. *Aerosol Sci. Technol.* **2012**, *46*, 1174−1186.

(51) Scarff, C. A.; Thalassinos, K.; Hilton, G. R.; Scrivens, J. H. Travelling Wave Ion Mobility Mass Spectrometry Studies of Protein Structure: Biological Significance and Comparison with X-Ray Crystallography and Nuclear Magnetic Resonance Spectroscopy Measurements. *Rapid Commun. Mass Spectrom.* **2008**, *22* (20), 3297−3304.